FAST WIDEBAND NEAR-FIELD IMAGING USING THE NON-EQUISPACED FFT WITH APPLICATION TO THROUGH-WALL RADAR

Michael Leigsnering and Abdelhak M. Zoubir

Signal Processing Group, Technische Universität Darmstadt
Merckstr. 25, 64283 Darmstadt, Germany
phone: + (49) 6151 16-2306, fax: + (49) 6151 16-3778, email: leigsnering@spg.tu-darmstadt.de
web: www.spg.tu-darmstadt.de

ABSTRACT

High resolution wideband near-field imaging requires wideband signals and large array apertures. Hence, a large amount of data needs to be processed in the image formation step. The standard delay and sum beamformer scales linearly with both output size and number of measurements resulting in high computational load. We propose a novel approach for image formation reducing the numerical complexity based on the non-equispaced fast Fourier transform (NFFT). The conventional delay and sum beamforming algorithm is reformulated such that the computational efficiency of the NFFT is exploited. Experimental results from a through-the-wall radar imaging system show a good improvement of the speed whereas the introduced error is kept very low.

1. INTRODUCTION

Various array signal processing applications, such as urban sensing [1, 2] or terahertz imaging [3] require wideband near-field beamforming or imaging. They have in common that sensor arrays and/or multiple measurements are used to reconstruct images of a scene of interest. Typically, high resolution images are desired to perform subsequent automated image analysis, e. g. segmentation and classification.

High resolution in the array plane (cross-range) and perpendicular to the array plane (downrange) calls for wideband large aperture systems. This results in a large number of measurements that need to be processed to form the output image. Existing approaches tackling the numerical complexity exploit assumptions such as far-field geometry or uniformly spaced linear arrays. However, if the focus delays are highly nonlinear these fast algorithms break down and one has to resort to the much more flexible backprojection [4, 5].

The standard backprojection or delay and sum beamforming approach requires $\mathcal{O}(QMN)$ evaluations of a complex exponential with subsequent weighted summation. Here, Q is the number of output pixels, M is the number of samples per sensor and N is the number of array elements. For high resolution images and large number of measurements this can be computationally very costly.

The formulation of the delay and sum beamformer has strong similarities to the discrete/fast Fourier transform (DFT/FFT). However, the nodes in the sum are not spaced regularly. In the end of the 1990s the concept of the FFT has been generalized to the so-called non-equispaced FFT (NFFT) [6, 7, 8]. The NFFT allows the fast approximate calculation of the DFT, when time and/or frequency nodes are non-equispaced.

We propose a novel approach which accelerates conventional delay and sum beamforming based on the NFFT. The standard beamformer equation is re-formulated such that the involved sums can be replaced by the NFFT. Hence, the computational efficiency of the NFFT is exploited for wideband near-field beamforming. It is shown that the numerical complexity is reduced to $\mathcal{O}(N(M\log M+|\log\varepsilon|Q))$, which is exponentially better than the classical backprojection approach.

In this paper, we focus on the application in through-the-wall radar imaging (TTWRI). The goal of this technology is to acquire detailed information of a scene using electromagnetic wave propagation that cannot be observed by other means. As TTWRI is designed for use in time critical situations, such as hostage crises or search and rescue missions, fast imaging results are vital. The diffraction of electromagnetic waves by the wall causes additional nonlinearities in the focus delays, thus backprojection is most suitable for TTWRI.

The theoretical considerations are supported by experimental TTWRI data results. For a reasonable amount of measurements and image size, we achieve a reduction in computational load by a factor of 40–50. At the same time the accuracy of the algorithm results in a PSNR of 50 dB or above. This precision is usually sufficient and can be further increased by trading off against speed.

In Section 2, we discuss the basic equations for wideband near-field beamforming. Furthermore, Section 3 introduces the concept of the NFFT. We present the proposed NFFT beamforming algorithm in Section 4. Finally, Sections 5 and 6 provide an assessment of the performance using experimental data and conclude the paper.

2. WIDEBAND NEAR-FIELD BEAMFORMING

The propagation of waves from a transmitter to the target and back to a receiver is subject to various distortions. The first order effects, the propagation delay and the reflection at the target, are modeled for subsequently deriving the image formation algorithm. The propagation delay depends on the scene geometry and the propagation medium. Whereas the reflection at the target results in an attenuation of the signal and/or a phase shift.

In the following, we consider wideband delay and sum beamforming (DSBF) for TTWRI as proposed in [5]. The proposed fast algorithms can, however, be applied to various imaging techniques or similar problems.

2.1 Received Signal Model

Aiming for a high downrange resolution, a wideband pulse must be used [5]. Assume that the wideband transceivers are placed on a physical or synthetic aperture array consisting of

N elements. In the stepped frequency approach the pulse is approximated by transmitting narrowband signals at discrete frequencies. Thus a finite number M of monochromatic signals with regular spaced frequencies f_m are used, covering the desired band, where $m = 0, 1, \ldots, M-1$.

The received signal model assumes that the region of interest can be described by P discrete targets with different reflectivities. Now the signal $y[m,n]$ at array element n and frequency f_m can be expressed as

$$y[m,n] = \sum_{p=0}^{P-1} \sigma_p w_m \exp(-j2\pi f_m \tau_{pn}), \tag{1}$$

where w_m is the weight of the m-th frequency, σ_p denotes the reflectivity of the p-th target and $n = 0, 1, \ldots, N-1$. If the wall parameters, i.e. the thickness and the permittivity, are known, the round-trip delay between the p-th target and the n-th receiver τ_{pn} can be calculated from geometric considerations. For the derivation of the delay for monostatic radar, see [5].

2.2 Delay and Sum Beamforming

The target region can be divided into a regular grid with finite number of pixels. Suppose the region of interest covers N_x and N_y points in crossrange and downrange, respectively. Using an appropriate numbering scheme, a single index q is sufficient for addressing all $N_x N_y = Q$ grid points (x_q, y_q), where $q = 0, 1, \ldots, Q-1$. For simplicity only a 2D target space is considered, however, the proposed approach can be straight forwardly extended to the 3D case.

By applying conventional DSBF, the beam can be steered at each pixel (x_q, y_q). The complex-valued image or B-scan can be obtained by [5]

$$I(x_q, y_q) = \frac{1}{MN} \sum_{n=0}^{N-1} \sum_{m=0}^{M-1} y[m,n] \exp(j2\pi f_m \tau_{qn}), \tag{2}$$

where τ_{qn} is the delay compensation for the n-th receiver steering the beam at position (x_q, y_q), M is the number of frequency bins and N is the number of array elements. It is noteworthy that the above equation employs wideband, near-field beamforming. Thus, the frequency dependent term cannot be factored out of the exponential and the function for the propagation delay τ_{qn} is highly non-linear. Assuming that the focus delays τ_{qn} are known and precomputed the numerical complexity of the conventional delay and sum beamforming algorithm is $\mathcal{O}(QMN)$.

3. THE NON-EQUISPACED FFT

The fast Fourier transform is a well known tool for vastly improving the speed of the DFT. However, the FFT requires the nodes in time and frequency domain to be uniformly spaced. The concept of the FFT has been generalized to arbitrary sampling situations where the nodes are not uniformly spaced; see [6, 7, 8]. There are numerous applications for this concept, e. g. in magnetic resonance imaging (MRI) [9] or computerized tomography [10].

In this work the C subroutine library NFFT 3.0 [11] as described in [12] was used as numeric implementation.

3.1 The Equispaced DFT/FFT

Following the standard notational conventions as in [12] the one dimensional (forward) DFT is defined as

$$z_l = \sum_{k=0}^{K-1} \hat{z}_k e^{-j2\pi kl/K}, \quad l = 0, \ldots, K-1, \tag{3}$$

where $K \in \mathbb{N}$, $\hat{z}_k \in \mathbb{C}$ are the given frequency coefficients and $z_l \in \mathbb{C}$ are the samples in time domain. The inverse DFT is now given by

$$\hat{z}_k = \frac{1}{K} \sum_{l=0}^{K-1} z_l e^{j2\pi kl/K}, \quad k = 0, \ldots, K-1.$$

The direct calculation of these transforms obviously require $\mathcal{O}(K^2)$ arithmetic operations, whereas the FFT needs only $\mathcal{O}(K \log K)$ to obtain the same result.

3.2 Definition of the Nonequispaced DFT

The definition of the forward DFT (3) can be generalized to the nonequispaced discrete Fourier transform (NDFT). Given the equispaced Fourier coefficients $\hat{z}_k \in \mathbb{C}, k = -\frac{K}{2}, \ldots, \frac{K}{2} - 1, K \in 2\mathbb{N}$, as input, the NDFT is defined as the evaluation of the corresponding trigonometric polynomial z at the set of L arbitrary nodes $a_l \in [-\frac{1}{2}, \frac{1}{2})$ [12]. This can be expressed as the sum

$$z_l = \sum_{k=-\frac{K}{2}}^{\frac{K}{2}-1} \hat{z}_k e^{-j2\pi k a_l}, \quad l = 0, \ldots, L-1. \tag{4}$$

In general the NDFT cannot be readily inverted. Thus, it is customary to define the adjoint NDFT [12]

$$w_k = \sum_{l=0}^{L-1} \hat{z}_l e^{j2\pi k a_l}, \quad k = -\frac{K}{2}, \ldots, \frac{K}{2} - 1.$$

Both transforms generally require $\mathcal{O}(KL)$ floating point operations. In most applications L is in the order of K and thus the evaluation is computationally expensive.

3.3 Efficient Computation

In order to improve computational efficiency of the NDFT fast approximation algorithms have been developed [6, 7, 8, 13]. These algorithms internally use an oversampled FFT together with a pre- and postprocessing step. In this fashion the numerical complexity of the NDFT can be significantly reduced while only slightly decreasing the accuracy of the computation.

The NFFT algorithm [12] employed in this paper achieves a good approximation result for the NDFT with only $\mathcal{O}(K \log K + |\log \varepsilon| L)$ operations. Here, ε is the desired accuracy of the computation. The accuracy can be controlled by an oversampling rate $\alpha \in \mathbb{R}$ and a window truncation parameter $r \in \mathbb{N}$. Generally, the approximatin accuracy and the computational load increase when increasing α or r.

3.4 Generalization

The concept of the NDFT (4) can be further generalized to the case where both time and frequency nodes are nonequispaced [8]. The transform is defined by

$$z_l = \sum_{k=0}^{K-1} \hat{z}_k e^{-j2\pi F v_k a_l}, \quad l = 0, \ldots, L-1, \tag{5}$$

where $v_k \in [-\frac{1}{2}, \frac{1}{2})$ are arbitrary frequencies and $F \in \mathbb{N}$ is the so-called nonharmonic bandwidth. The fast implementation of this transform is referred to as fast Fourier transform for nonequispaced data in space and frequency domain (NNFFT) [12] or as type 3 nonuniform FFT [14]. The NNFFT takes $\mathcal{O}(F \log F + |\log \varepsilon|(K+L))$ operations to compute.

4. FAST BEAMFORMING USING THE NONEQUISPACED FFT

Observing the formulation of the conventional delay and sum beamformer (2) we reformulate the problem in order to apply the NFFT. First we decompose the DSBF to sub-images $I_n(x_q, y_q)$ based on the measurements of sensor n only

$$I(x_q, y_q) = \frac{1}{MN} \sum_{n=0}^{N-1} I_n(x_q, y_q). \tag{6}$$

Subsequently, the sums for the sub-images are modified to obtain an expression matching the NDFT

$$\begin{aligned} I_n(x_q, y_q) &= \sum_{m=0}^{M-1} y_n[m] \exp\left(j2\pi f_m \tau_{qn}\right) \\ &= \sum_{m=-M/2}^{M/2-1} y_n[m] \exp\left(j2\pi (f_c + m\Delta f)\tau_{qn}\right) \\ &= e^{j2\pi f_c \tau_{qn}} \cdot \sum_{-m=M/2}^{M/2-1} y_n[m] \exp\left(j2\pi m \Delta f \tau_{qn}\right) \\ &= e^{j2\pi f_c \tau_{qn}} \cdot \underbrace{\sum_{-m=M/2}^{M/2-1} y_n[m] \exp\left(-j2\pi m(-\Delta f \tau_{qn})\right)}_{\text{Can be calculated using the NDFT/NFFT}}, \end{aligned} \tag{7}$$

where f_c is the center frequency and Δf is the frequency step width.

The reformulated DSBF can be calculated efficiently using the NFFT. In this fashion the required operations decrease to $\mathcal{O}(N(M \log M + |\log \varepsilon| Q))$ as N evaluations of the NFFT are performed.

4.1 Fast Calculation of the Measurement Equation

Using similar reformulations as above one can find a fast method for evaluating the measurement equation (1) using the adjoint NDFT/NFFT. Many iterative optimization algorithms require the alternating calculation of the predicted measurements and the beamforming result, e. g. compressive sensing approaches [15]. These methods benefit from a fast evaluation of the measurement equation.

4.2 Fast Beamforming with Sparse Frequency Measurements

In some applications, one may not use uniformly spaced frequency measurements around a certain center frequencies, but the frequencies are rather irregularly spaced. E. g. when applying compressive sensing, using a random subset of the uniformly spaced frequencies is beneficial. In this case, it is possible to use the NNFFT (5) for the fast generation of the beamformed image.

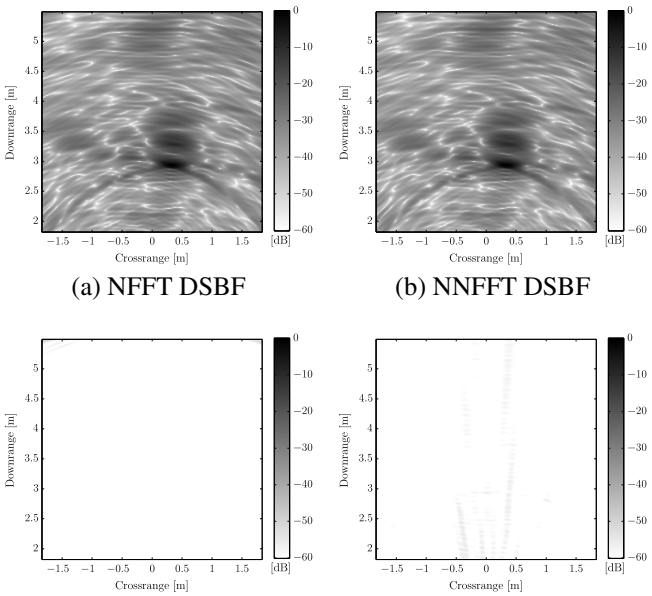

(a) NFFT DSBF (b) NNFFT DSBF

(c) Residuals of NFFT DSBF (d) Resid. of NNFFT DSBF

Figure 1: Images (a) and (b) show B-scans of the single sphere scene applying the fast beamforming algorithms. See (c) and (d) for the residuals as compared to conventional DSBF

The expression for the sub-images (7) can be rewritten as

$$I_n(x_q, y_q) = \underbrace{\sum_{m=0}^{\tilde{M}-1} y_n[m] \exp\left(j2\pi F \tilde{f}_m \tilde{\tau}_{qn}\right)}_{\text{Can be calculated using the NNFFT}},$$

where $\tilde{M}$ is the number of frequency bins, $c_1 \cdot f_m = \tilde{f}_m \in [-\frac{1}{2}, \frac{1}{2}), c_2 \cdot \tau_{qn} = \tilde{\tau}_{qn} \in [-\frac{1}{2}, \frac{1}{2})$ are scaled versions of the respective variable without a tilde. For the nonharmonic bandwidth F and the scaling constants $c_1, c_2 \in \mathbb{R}$ the following conditions must hold

$$c_1 c_2 F = 1, \quad F \in \mathbb{N}.$$

The smallest possible F should be chosen in order to minimize computational cost.

The fast implementation of the DSBF on sparse frequency data only needs $\mathcal{O}(N(F \log F + |\log \varepsilon|(Q + \tilde{M})))$ floating point operations. This results from one NNFFT computation for each of the N sensors.

Using the adjoint NNFFT, the measurement equation (1) can be quickly computed for irregularly spaced frequencies.

5. EXPERIMENTAL RESULTS

The measurements were acquired using a TTWRI system in an anechoic chamber with a reflective floor. A uniformly spaced square array with 57 $\times$ 57 elements having an element spacing of 2.2 cm is placed in front of a concrete wall at a distance of 1.05 m. From each element, 801 monofrequent measurements are taken equally spaced from 700 MHz to 3.1 GHz. The center of the array is 1.22 m above the floor. The wall parameters, wall thickness $d = 14.3$ cm and relative

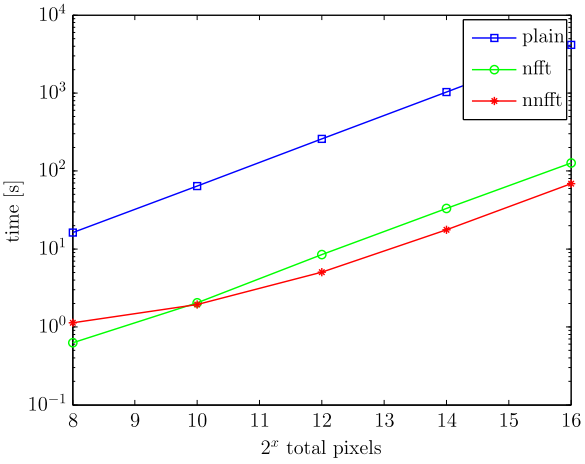

Figure 2: Computation time vs. total number of pixels in output image

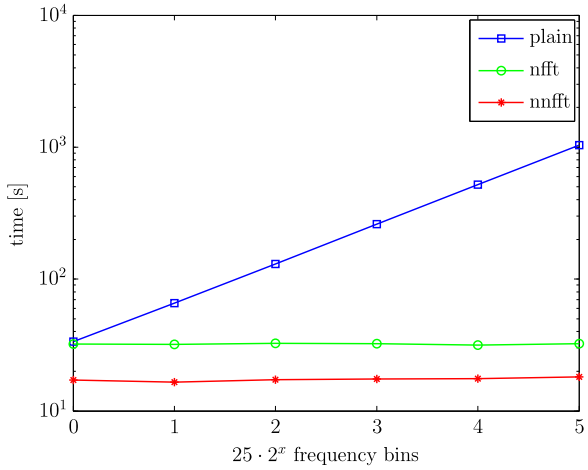

Figure 3: Computation time vs. number of frequency bins

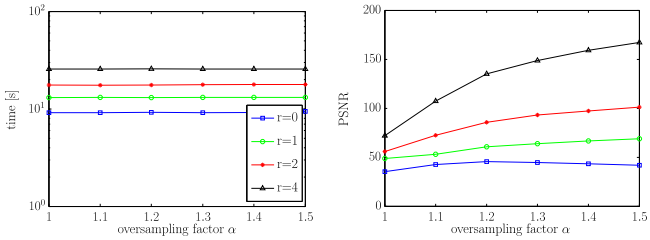

(a) (b)

Figure 4: Computation time and PSNR vs. oversampling rate α and window length r for the NNFFT approach.

permittivity $\varepsilon_r = 7.6632$, are known. Behind the wall a single sphere (diameter of 25 cm) is placed on a foam column with height 1.2 m. The considered B-scan cut is taken at a height of 18 cm above the array center which is approximately the middle of the sphere. In Figure 1 two examples B-scans and the respective residuals are depicted.

In order to evaluate the savings in terms of numerical complexity, two different scenarios have been considered. For both scenarios 1500 array elements were chosen randomly to reduce the image generation time. As for all algorithms the time will scale linearly with the number of array elements the dependency on this parameter was not evaluated numerically. For all near-field wide band beamforming algorithms it was assumed that the focus delays τ_{qn} were calculated and stored beforehand. The computations were carried out in MATLAB(tm) C-mex functions on a work station with 3.1 GHz AMD Phenom(tm) II X2 550 Processor in single threaded mode.

In the first scenario, the number of frequency bins was fixed to $M = \tilde{M} = 801$ and the size of the output image was varied. The number of output pixels Q was set to $16 \times 16 = 2^8, 2^{10}, \ldots, 2^{16}$. For each image the straight forward DSBF method and the two proposed efficient approaches were evaluated. For the approximation algorithms the parameters were chosen such that the PSNR stays in the order of 50 dB. The running time is shown on a log-log scale in Figure 2.

As expected, the plain DSBF algorithm scales according to Q. For the NFFT implementation the computation time scales accordingly due to the $|\log \varepsilon| Q$ term dominating the complexity order. In the case of the NNFFT the running time has a flat start as $\tilde{M} > Q$ in this region. For a larger number of pixels, Q dominates in $|\log \varepsilon|(Q + \tilde{M})$, hence the implementation scales according to the other methods. It is evident that the constant involved in the complexity is about 40-50 times for the (N)NFFT implementations and thus a good performance improvement is achieved.

In the second scenario the size of the output image was fixed to $Q = 128 \times 128 = 2^{14}$ and the number of frequency bins was varied. The frequency bins were subsampled by a factor of $1, 2, \ldots, 2^5$. Again, the three different algorithms were evaluated. For the approximation algorithms, the PSNR was 50 dB or better except for the case where only 25 frequencies were used. The running time is shown on a log-log scale in Figure 3.

The plain DSBF algorithm scales linearly with the number of frequency bins M as well. However, in this scenario the approximation algorithms show a different behavior. For both NFFT and NNFFT the computation time remains constant with increasing number of frequencies. This is due to their complexity depending on the sum of the number of frequency bins and pixel (disregarding the constants) rather than the product of the both. This results in a good performance improvement for a realistic number of frequencies of 400 to 800.

Furthermore, the approximation accuracy of the proposed methods is evaluated. In both of the above scenarios, the NNFFT algorithm performs slightly better than the NFFT algorithm. Having the additional advantage of being more flexible only the NNFFT approach will be considered in the following study.

The image size was set to $Q = 128 \times 128 = 2^{14}$ and the number of frequency bins was fixed to $M = \tilde{M} = 801$. Two approximation parameters of the NNFFT algorithm were considered. Firstly, the oversampling factor α and and secondly the window truncation length r. The computation time and the PSNR are depicted in Figure 4 for a reasonable parameter range according to [12].

It can be observed that the computation time solely depends on the choice of r in the given scenario. For a choice of $r = 1, 2$ the PSNR is well above 50 dB which should be

sufficient for most applications. Hence, this is a good trade-off between speed and accuracy. Increasing the oversampling factor α slightly improves the PSNR as well. As there is no additional computational cost involved it is beneficial to chose a large α.

6. CONCLUSION

A novel application of the (N)NFFT in order to accelerate wideband near-field delay and sum beamforming has been presented. By exploiting the structure of the beamforming equation an efficient implementation was proposed. Using experimental data the numerical efficiency was shown to be improved by a factor of 40 to 50 while keeping the PSNR in a very good range.

ACKNOWLEDGEMENT

The authors would like to thank Prof. Dr. Moeness Amin and Dr. Fauzia Ahmad from the Center of Advanced Communications at Villanova University, Villanova, PA, USA, for providing the experimental data.

REFERENCES

[1] M. Amin, editor. *Through-the-Wall Radar Imaging*. CRC Press, 2010.

[2] C. Debes, M. Amin, and A. Zoubir. Target detection in single- and multiple-view through-the-wall radar imaging. *IEEE Transactions on Geoscience and Remote Sensing*, 47(5):1349–1361, 2009.

[3] A. Bandyopadhyay, A. Stepanov, B. Schulkin, M. D. Federici, A. Sengupta, D. Gary, J. F. Federici, R. Barat, Z.-H. Michalopoulou, and D. Zimdars. Terahertz interferometric and synthetic aperture imaging. *J. Opt. Soc. Am. A*, 23(5):1168–1178, May 2006.

[4] J. A. Fawcett. Inversion of n-dimensional spherical averages. *SIAM Journal on Applied Mathematics*, 45(2):336–341, 1985.

[5] F. Ahmad and M. Amin. Multi-location wideband synthetic aperture imaging for urban sensing applications. *Journal of the Franklin Institute*, 345(6):618 – 639, 2008.

[6] G. Beylkin. On the fast Fourier transform of functions with singularities. *Applied and Computational Harmonic Analysis*, 2(4):363–381, 1995.

[7] A. Dutt and V. Rokhlin. Fast Fourier transforms for nonequispaced data, II. *Applied and Computational Harmonic Analysis*, 2(1):85–100, 1995.

[8] D. Potts, G. Steidl, and M. Tasche. *Fast Fourier transforms for nonequispaced data: A tutorial*, chapter 12, pages 247–269. Birkhäuser, 2001.

[9] H. Eggers, T. Knopp, and D. Potts. Field inhomogeneity correction based on gridding reconstruction for magnetic resonance imaging. *IEEE Transactions on Medical Imaging*, 26(3):374–384, 2007.

[10] D. Potts and G. Steidl. New Fourier reconstruction algorithms for computerized tomography. In *Proceedings of SPIE*, volume 4119, page 13, 2000.

[11] J. Keiner, S. Kunis, and D. Potts. NFFT 3.0, C subroutine library. `http://www-user.tu-chemnitz.de/~potts/nfft`, 2006.

[12] J. Keiner, S. Kunis, and D. Potts. Using NFFT 3—a software library for various nonequispaced fast fourier transforms. *ACM Trans. Math. Softw.*, 36:19:1–19:30, August 2009.

[13] J. Fessler and B. Sutton. Nonuniform fast fourier transforms using min-max interpolation. *Signal Processing, IEEE Transactions on*, 51(2):560 – 574, Feb. 2003.

[14] J. Lee and L. Greengard. The type 3 nonuniform FFT and its applications. *Journal of Computational Physics*, 206(1):1–5, 2005.

[15] M. Leigsnering, C. Debes, and A. Zoubir. Compressive sensing in through-the-wall radar imaging. IEEE International Conference on Acoustics, Speech and Signal Processing, May 2011. accepted.